RESEARCH ARTICLE

Key Points:
- Aerosol effects on the diurnal cycle of precipitation and lightning are investigated
- Aerosols tend to cause more and delayed heavy precipitation and lightning
- Aerosol radiative effect delays the occurrence of strong convection

Correspondence to:
J. Guo,
jpguocams@gmail.com

Delaying precipitation and lightning by air pollution over the Pearl River Delta. Part I: Observational analyses

Jianping Guo[1], Minjun Deng[1], Seoung Soo Lee[2], Fu Wang[3], Zhanqing Li[2], Panmao Zhai[1], Huan Liu[1], Weitao Lv[1], Wen Yao[1], and Xiaowen Li[4]

[1]State Key Laboratory of Severe Weather, Chinese Academy of Meteorological Sciences, Beijing, China, [2]Department of Atmospheric and Oceanic Sciences and Earth System Science Interdisciplinary Center, University of Maryland, College Park, Maryland, USA, [3]National Satellite Meteorological Center, Beijing, China, [4]School of Geography, Beijing Normal University, Beijing, China

Abstract The radiative and microphysical effects of aerosols can affect the development of convective clouds. The objective of this study is to reveal if the overall aerosol effects have any discernible impact on the diurnal variations in precipitation and lightning by means of both observational analysis and modeling. As the first part of two companion studies, this paper is concerned with analyzing hourly PM_{10}, precipitation, and lightning data collected during the summers of 2008–2012 in the Pearl River Delta region. Daily PM_{10} data were categorized as clean, medium, or polluted so that any differences in the diurnal variations in precipitation and lightning could be examined. Heavy precipitation and lightning were found to occur more frequently later in the day under polluted conditions than under clean conditions. Analyses of the diurnal variations in several meteorological factors such as air temperature, vertical velocity, and wind speed were also performed. They suggest that the influence of aerosol radiative and microphysical effects serve to suppress and enhance convective activities, respectively. Under heavy pollution conditions, the reduction in solar radiation reaching the surface delays the occurrence of strong convection and postpones heavy precipitation to late in the day when the aerosol invigoration effect more likely comes into play. Although the effect of aerosol particles can be discernible on the heavy precipitation through the daytime, the influence of concurrent atmospheric dynamics and thermodynamics cannot be ruled out.

1. Introduction

Aerosols influence the atmospheric radiative budget and the global hydrologic cycle through their direct and indirect effects [*Forster et al.*, 2007; *Tao et al.*, 2012; *Rosenfeld et al.*, 2014]. Aerosols can directly influence the energy balance of the earth-atmosphere system by scattering and absorbing solar radiation. Aerosol particles can also alter cloud microphysical processes and affect precipitation by acting as cloud condensation nuclei (CCN) [*Albrecht*, 1989; *Twomey*, 1977] or as ice nuclei [*Levin and Cotton*, 2009]. Observations and model simulations of the aerosol indirect effect on precipitation and lightning, in particular, has been the focus of many recent studies [*Rosenfeld et al.*, 2008; *Wang et al.*, 2011; *Yuan et al.*, 2011, 2012; *Fan et al.*, 2013; *Guo et al.*, 2014a; *Yang and Li*, 2014].

Increases in aerosol loading appear to be associated with the invigoration of deep convective clouds, leading to more frequent episodes of heavy precipitation [*Zhang et al.*, 2007; *Li et al.*, 2011; *Koren et al.*, 2012]. Other studies have reported that greater aerosol loading leads to suppressed convective activity and heavy precipitation events [*Rosenfeld*, 1999; *Givati and Rosenfeld*, 2004]. The overall net effects have yet to be identified, let alone quantified [*Li et al.*, 2011]. Broadly speaking, the aerosol effect can be further divided into microphysical and radiative effects. These effects can cancel each other out during the precipitation forming process depending on the aerosol concentration, aerosol optical properties, and the moisture supply [*Koren et al.*, 2008]. In a moist and convectively unstable environment, higher aerosol concentrations tend to invigorate convective precipitation by increasing the vertical transport of water in the form of smaller droplets to altitudes where additional latent heat is released by the freezing of water [*Rosenfeld et al.*, 2008].

Lightning is a cloud electrification phenomenon which mostly occurs when clouds develop swiftly to high altitudes above the freezing level and ice particles collide in the presence of supercooled liquid [*Saunders*, 1994]. Earlier laboratory studies indicated that the supercooled liquid is necessary for appreciable charge

separation during rebounding collisions between small ice and riming graupel [e.g., *Takahashi*, 1978; *Jayaratne*, 1993; *Baker and Dash*, 1994]. Not all clouds that generate lightning are tall or extend to great distances above the freezing level. For instance, slantwise convection associated with baroclinic systems in storm track regions such as those containing the Gulf Stream and the Kuroshio Extension produces a considerable amount of lightning [*Christian et al.*, 2003].

The role of aerosol pollution in elevating storm heights and enhancing lightning activity was confirmed over the western Pacific Ocean to the east of the Philippines [*Yuan et al.*, 2011]. The number of lightning flashes was found to increase with increasing aerosol loading [*Avila et al.*, 1999; *Altaratz et al.*, 2010] and so did the storm and lightning heights. The finding of midweek peak in lightning is another indicator for the enhancement effect of aerosols that is particularly strong under humid and convectively unstable environments [*Bell et al.*, 2009]. More recent studies have indicated aerosols being but one environmental factor that can influence deep convective clouds and lightning and alter cloud radiative forcing [e.g., *Storer et al.*, 2014; *Wall et al.*, 2014; *Peng et al.*, 2015; *Stolz et al.*, 2015]. On the other hand, the radiative effect of absorbing aerosols leads to heating of the atmospheric layer and to cooling of the surface, thereby reducing latent heat fluxes and stabilizing the atmosphere. As a consequence, clouds, convection, and electrical activity are likely to be inhibited [*Koren et al.*, 2004]. Conversely, the invigoration effect of absorbing aerosols on storm activity and lightning is often observed. For instance, biomass burning aerosols produced in Mexico have been found to be positively associated with the occurrence of severe weather (hail and lightning) offshore of Mexico [*Kucienska et al.*, 2012] and over the downwind central U.S. region [*Lyons et al.*, 1998; *Wang et al.*, 2009]. The microphysical effects of smoke particles on clouds were hypothesized to be one of the main factors behind this. This observed aerosol invigoration effect could be due to the fact that precipitation development by warm rain processes is stunted and cloud liquid is then transported to higher latitudes to participate in riming processes and thus infer cold-rain microphysical processes. This in turn leads to a greater release of latent heat and invigorated updrafts, facilitating the development of intense thunderstorms and large hail [*Rosenfeld*, 1999; *Andreae et al.*, 2004].

To our knowledge, observation-based studies investigating the effect of absorbing aerosols on thermodynamic profiles are few and far between. Reanalysis data sets that incorporate new aerosol retrieval climatologies and that account for the presence of scattering/absorbing aerosols in the radiative transfer calculation have recently been developed [*Dee et al.*, 2011]. They have led to improved simulations of the African easterly jet, a better representation of the North African monsoon [*Tompkins et al.*, 2005], more accurately predicted tropical precipitation amounts, and a reduction in mean extratropical circulation errors [*Rodwell and Jung*, 2008]. Therefore, the direct radiative effect of aerosols can be profound and cannot be ignored at all.

Many studies concerning the diurnal variations in precipitation and lightning have been published [*Wallace*, 1975; *Fujibe*, 1999; *Hidayat and Ishii*, 1999; *Walters and Winkler*, 1999; *Basu*, 2007]. Few have associated the diurnal variations with the aerosol indirect effect on an hourly time scale. *Fan et al.* [2013] have simulated the diurnal variations in clouds and precipitation under varying aerosol concentration conditions. They have found that an increase in aerosol loading tends to delay the occurrence of convective clouds, but no observational analyses were performed to support the modeling results. The anthropogenic aerosol effect on the weekly cycle of convective precipitation can be detected, depending on the geographical location [*Bäumer and Vogel*, 2007; *Rosenfeld and Bell*, 2011], suggesting that other nonaerosol-related factors play roles in the weekly cycle [*Bell et al.*, 2009]. Still, aerosol-induced changes in heavy precipitation and lightning on an hourly time scale are far from understood. Therefore, we focus on this problem in the current study.

Due to the extraordinarily rapid economic development in recent decades, eastern China, and the Pearl River Delta (PRD) region in particular, severe atmospheric pollution has plagued the region [*Qian et al.*, 2006; *Guo et al.*, 2011]. Under the influence of the summer monsoon climate, lightning and heavy precipitation frequently strike southeastern China, including the PRD region, in summer. The lightning frequency over this region observed from space is much more than over other regions at the same latitude [*Christian et al.*, 2003]. *Wang et al.* [2011] have found that simultaneous maxima in thunderstorm activity and air pollution level in the PRD region occur frequently. Motivated by the observed concurrent variations in aerosols and lighting/heavy precipitation in the PRD region, the goal of this study is to examine the diurnal variations in storms, lightning, and anthropogenic aerosols in the region and to determine whether aerosols have any impact on the diurnal variation in thunderstorms using hourly observations. A companion paper (Lee et al., in review at J. Geophys. Res.—Atmos., 2016, hereafter Part II) aims to gain a better understanding of the mechanisms using a cloud-system resolving model (CSRM).
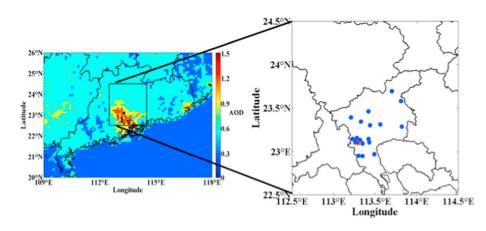
Figure 1. Location of the study area (22.5°N–24.5°N, 112.5°E–114.5°E). (left) The spatial distribution of mean summertime (June through August) MODIS AOD averaged over 2008–2012. (right) Locations of the 19 air quality observation stations (blue dots). The red triangle in Figure 1 (right) shows the location of Guangzhou (23.1°N, 113.3°E).

2. Data and Methods

2.1. The Study Region

The study region (22.5°N–24°N, 112.5°E–114.5°E) is characterized by relatively warm and moist atmospheric conditions during the summer months. Frequent heavy precipitation events and severe anthropogenic pollution episodes are typical over this region of southeastern China during this time of year [*Guo et al.*, 2011]. *Fu and Dan* [2014] have reported that the number of medium to heavy precipitation events have increased slightly over the past 50 years in southern China.

Figure 1 shows the spatial distribution of mean aerosol optical depth (AOD) from the Moderate Resolution Imaging Spectroradiometer (MODIS) on board the Aqua spacecraft over the study region during the summer months of 2008–2012. Aerosol pollution over the PRD region is more severe than over neighboring regions. Nineteen stations measuring primary atmospheric pollutants on an hourly basis are also located in the study region (Figure 1, right).

2.2. Data

An observational air quality network was established and is maintained by the Guangzhou Environmental Protection Bureau. Hourly air quality data sets collected in June, July, and August of 2011 and 2012 at the 19 stations comprising the network are used in the study. Quantities measured include particulate matter up to 10 μm in size (PM_{10}) and nitrogen dioxide (NO_2). Although satellite-derived AOD has been used as a proxy for CCN [*Andreae*, 2009], the most serious problems encountered when using the MODIS AOD are that it is only measurable under cloud-free conditions and that it gives no information about where aerosols reside in the vertical column. Other challenges exist when trying to obtain coincident measurements of aerosols and precipitation necessary for the study of aerosol-induced changes in the precipitation diurnal cycle proposed here. Spaceborne AOD retrievals are inevitably susceptible to humid swelling [*Twohy et al.*, 2009] and the retrievals themselves are prone to various errors as critically reviewed by *Li et al.* [2009].

Given the above problems, we choose to use ground measurements of PM_{10} concentration which are available under all-sky conditions. While it would be better to use particulate matter up to 1 μm in size (PM_1) and 2.5 μm in size ($PM_{2.5}$) [*Seinfeld and Pandis*, 1998], much fewer such data are available for matching with precipitation data. Using a recent year (November 2013 to October 2014) of coincident $PM_{2.5}$ and PM_{10} measurements at the Guangzhou station, we found a good correlation ($R = 0.95$ in summer) between them, as shown in Figure 2. Since this study is concerned with the qualitative assessment of the potential effect of aerosols on the diurnal variation in precipitation, PM_{10} is chosen as a proxy for CCN instead, which is sufficient for our needs. Because aerosol particles are generally well mixed in the boundary layer, PM_{10} data can indicate the occurrence of major aerosol episodes over the relatively small domain covered by the PRD region. *Anderson et al.* [2003] have shown that the variability in aerosol properties at such a spatial scale is not very large. However, we concede that using PM_{10} as a proxy for CCN opens up the potential for confounding aerosol-precipitation
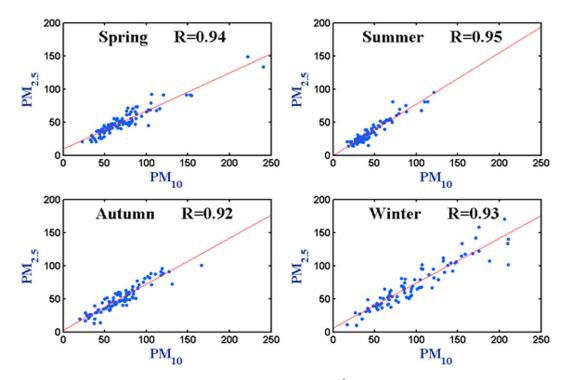
Figure 2. The scatterplots of daily PM$_{2.5}$ concentrations (in units of $\mu g\, m^{-3}$) as a function of coincident daily PM$_{10}$ concentrations in spring, summer, autumn, and winter at the Guangzhou station.

interactions because of the presence of a very small number of supermicron-sized CCN over the PRD region and the presence of sea spray-induced salt CCN (giant CCN or GCCN) over the neighboring South China Sea. Both kinds of particles could lead to efficient warm rain processes, given (1) the ability of these particles to readily activate at supersaturation levels commonly achieved near the cloud bases of deep cumulonimbi and (2) the great availability of small droplets (resulting from the generally high CCN concentrations) for collection.

Temporal homogeneity tests were applied to PM$_{10}$ measurements from all sites [*Feng et al.*, 2004]. A further requirement is that greater than 95% of the total number of days of measurements over the two summer seasons at each station must contain a complete set of hourly measurements. All 19 sites passed these quality control checks, so all air pollution data from these sites are used in this study.

Rain gauge measurements and satellite estimates of precipitation cannot completely reflect the true diurnal cycle of precipitation. For example, the Climate Prediction Center MORPHing (CMORPH)-retrieved precipitation peaks generally lag 0–12 h behind those seen in rain gauge data [*Guo et al.*, 2014a]. Although there are many automatic weather stations (AWS) deployed in China, data from these stations cannot fully describe precipitation features, especially in areas with complex terrain. Fortunately, the China Meteorological Information Center of the China Meteorological Administration has developed a new generation precipitation product that merges AWS rain gauge data with CMORPH rain rates [*Shen et al.*, 2014]. The quality of the hourly gridded (0.1° × 0.1°) precipitation product over China has been widely validated and has been shown to be an improvement over the previous CMORPH product. The data set was therefore used in this study.

The China Lightning Location Network (CLLN) is based on the time-of-arrival/direction-finder combined technique using very low frequency sferics. Each lightning detection sensor records lightning radiation at 30 kHz with a bandwidth of several kHz. The CLLN routinely reports the time, position, polarity, and peak current of the first stroke in each detected cloud-to-ground (CG) flash. A postprocessing algorithm is then used to group individual strokes into flashes. Observations from the CLLN have been widely used for lightning warning and severe weather monitoring since the 1990s [*Chen et al.*, 2011]. Currently, there are 14 CLLN sites in the PRD region. The only current reliable method for locating lightning is through triangulation, i.e., using at least three antennas. This often leads to the rejection of cloud-to-cloud (CC) lightning flashes because one antenna detects the position of the flash on the starting cloud, while the other detects it on the receiving cloud. The CLLN can only provide the positions of CG flashes except for reliably detected CC and intracloud flashes. As a

result, the CLLN tends to underestimate the number of flashes, especially at the beginning of storms when CC lightning is prevalent. As such, we only consider CG flashes and their association with aerosols and NO_2. According to the pioneering work done by *Meng et al.* [2006], the detection efficiency of the lightning detectors used in the CLLN is typically ~90% with a location accuracy of 500 m. This relatively high detection performance provides enough reliable CG lightning data to study the diurnal cycle of lightning, including positive CG (PCG) and negative CG (NCG) lightning.

Diurnal variations in precipitation, lightning, and air pollutant concentrations over the PRD region are closely related to large-scale synoptic conditions, which is likely one of the key factors resulting in contradictory findings regarding the magnitude, and even the sign, of aerosol-induced changes in precipitation [*Tao et al.*, 2012]. The covariability between aerosols, precipitation, and other meteorological factors has been explicitly examined [*Huang et al.*, 2009], although disentangling meteorological effects from aerosol effects remains a daunting task. To tease out the aerosol contribution to the precipitation and lightning features with respect to meteorological conditions, ERA-Interim Reanalysis data from the European Centre for Medium-Range Weather Forecasts (ECMWF) [*Uppala et al.*, 2008] were used to examine the diurnal variations in local-scale circulation over the PRD region.

From a statistical point of view, the Tropical Rainfall Measuring Mission (TRMM) data allow for characterization of the diurnal cycle over many days/overpasses, due to their close association with the development of and diurnal variation in deep convection [*Liu and Zipser*, 2008; *Liu et al.*, 2010] compared with ones derived from reanalysis data. On the other hand, the individual snapshots of TRMM do little to achieve this goal. Even though reanalysis products have their own inherent assumptions, parameterizations, and errors, the spatiotemporal coverage of these products is the best we can work with in an "observational" study such as this one. Numerous studies involving the aerosol indirect effect on precipitation [e.g., *Fan et al.*, 2009] have indicated that factors such as lower tropospheric stability (LTS), vertical velocity (ω), and vertical wind shear from reanalysis data can be used to determine regions favorable for the development of deep convection. Therefore, data used in this study include air temperature (for the derivation of LTS), ω, and wind speed (for the derivation of vertical wind shear), which will be described in detail in section 2.3. The ERA-Interim data set has 37 vertical levels ranging from 1000 hPa to 1 hPa, with a horizontal spatial resolution of $0.125° \times 0.125°$ and a 6-hourly temporal resolution. Data are output at four time points during the day (0000, 0600, 1200, and 1800 Coordinated Universal Time, or UTC).

2.3. Methodology

All data sets were resampled to create a grid containing $0.5° \times 0.5°$ grid boxes of collocated aerosol-precipitation-lightning data covering the PRD region. All data are recorded in UTC. Given the potential effect of solar radiation on the diurnal cycle of precipitation, the UTC time unit was converted to local solar time, i.e., Beijing time (BJT), using the following equation:

$$BJT = UTC + 8. \tag{1}$$

The mean precipitation amount for a specific hour was calculated by averaging the precipitation amount in all the grid boxes over the PRD region at that specific hour during the five consecutive summer seasons. When the mean precipitation amount is greater than 0 mm at a given hour, this is called a precipitation case. Following methods developed by *Sorooshian et al.* [2002] and *Guo et al.* [2014b], the region-averaged mean precipitation at the tth hour for the dth day over the PRD expressed as $r(t, d)$ is calculated by averaging rainfall over all $0.5° \times 0.5°$ grid boxes. Then the region-averaged precipitation amount at the tth hour, expressed as $\overline{P}(t)$, is calculated by averaging $r(t, d)$ over the 460 days compiled over the five consecutive summer seasons in the PRD region. A time series of average hourly precipitation amount, which is further examined to identify the maximum in precipitation amount (amplitude) and the preferred time of occurrence (phase) on a particular day, is obtained. Anomalies were calculated as the amplitude minus the 24 h mean [*Wallace*, 1975; *Yu et al.*, 2007]. The amplitude anomaly is given in units of percent, which provides a measure of the magnitude of the diurnal cycle with respect to the 24 h mean precipitation amount. For example, an amplitude anomaly of 100% means that the magnitude of the maximum amount of precipitation is twice that of the 24 h mean.

The occurrence frequency of precipitation at a given hour is the total cumulative number of hours with rainfall. Individual rainfall events are defined for each 1 h period when the domain-averaged precipitation exceeds 0 mm. As a result, the number of rainfall occurrences at this hour is compiled once. Therefore, diurnal

Table 1. Statistics Describing Clean and Polluted Conditions in Terms of Daily Mean PM_{10} Concentrations

	Bottom Tercile (≤33.3%)	Top Tercile (≥66.7%)
Daily mean PM_{10}	$10 \sim 42\ \mu g\ m^{-3}$	$57 \sim 149\ \mu g\ m^{-3}$
Atmospheric condition	Clean	Polluted
Number of days	159	157

cycles in precipitation amount and frequency can be explicitly calculated over the PRD region. The lightning density refers to the average number of lightning strikes to the ground detected over all $0.5° \times 0.5°$ grid boxes at a particular hour during the five summer seasons of 2008–2012. Lightning need not be detected in each grid box for this calculation. If the domain mean lightning density is greater than $0\ flash\ h^{-1}\ km^{-2}$, the number of lightning (including CG, PCG, and NCG) flashes for this hour is compiled once, i.e., one observation of the frequency of occurrence of lightning is compiled. In this way, diurnal cycles of lightning density and frequency can be determined as well. PM_{10}, NO_2, and other variables are likewise treated in the way described above. All diurnal variations are normalized to facilitate comparisons made among different variables. Note that statistics regarding precipitation, lightning, PM_{10}, NO_2, and other variables are domain averages unless specified otherwise.

Given that precipitation can wash out the atmospheric particles [*Huang et al.*, 2009], caution should be exercised when we use coincident hourly PM_{10} and precipitation data to study the possible impact of air pollution on diurnal variations of precipitation. All summertime daily PM_{10} data were firstly sorted and then divided into three categories with each category containing an equal number of samples. The highest tercile of daily PM_{10} concentration was labeled as the polluted case and the lowest tercile was labeled as the clean case. Dividing all data into three equal-sized subsets can create sufficient contrast between the subsets and can ensure smaller standard deviations for each subset. The criteria for defining polluted and clean conditions are summarized in Table 1. In a similar manner, hourly precipitation measurements were divided into three similar categories: light, medium, and heavy precipitation.

The bottom and top terciles of all sorted hourly precipitation data were calculated so that the precipitation intensity, i.e., light or heavy, could be determined (Table 2). Figure 3 shows the PDFs and accumulated occurrence frequencies of PM_{10} concentration and hourly rain rate. The number of days of daily mean PM_{10} data is 159 and 157 for the bottom and top terciles, respectively. Thresholds of PM_{10} concentrations for the two terciles are $42\ \mu g\ m^{-3}$ and $57\ \mu g\ m^{-3}$, respectively. Daily mean PM_{10} concentrations less than $42\ \mu g\ m^{-3}$ or greater than $57\ \mu g\ m^{-3}$ define a clean day and a polluted day, respectively. The total number of hours comprising the hourly mean rainfall data set in the bottom and top terciles is 1584 h each. Light precipitation conditions are associated with hourly mean rainfall rates of $< 0.04\ mm\ h^{-1}$ and heavy precipitation conditions are associated with hourly mean rainfall rates of $0.35–20\ mm\ h^{-1}$. Note that caution should be exercised when the thresholds for categorizing heavy precipitation are extended to other regions.

Variations in hourly mean precipitation amount, precipitation/lightning occurrence frequency, heavy (light) precipitation frequency, and PCG/NCG lightning frequency under clean and polluted conditions were examined. Probability distribution functions (PDF) of the number of hours with heavy precipitation under clean and polluted conditions were investigated as well, with a focus on the second half of the day (1200–2400 BJT). The last half of the day was chosen because this is when precipitation events are most likely to occur.

Since diurnal cycles of precipitation and lightning are subject to variations in large-scale (synoptic) atmospheric conditions, diurnal variations in meteorological factors are examined as well. A myriad of factors dictating the influence of aerosols on precipitation have been identified [*Koren et al.*, 2010; *Tao et al.*, 2012]. As a first step in determining if key meteorological variables have experienced the same diurnal variation as aerosols, three most widely recognized atmospheric factors are analyzed, namely, LTS, ω, and vertical wind shear [*Fan et al.*, 2009; *Zhang et al.*, 2014].

LTS describes the thermodynamical state of the troposphere [*Wood and Bretherton*, 2006] and is defined as the differences in potential temperature, θ, between the free troposphere (700 hPa) and the surface (LTS $= \theta_{700hPa} - \theta_{1000hPa}$) [*Slingo*, 1987]. Biases in low-level temperature are known to exist in reanalysis data,

Table 2. Statistics Describing Light and Heavy Precipitation Events in Terms of Hourly Mean Precipitation Amounts

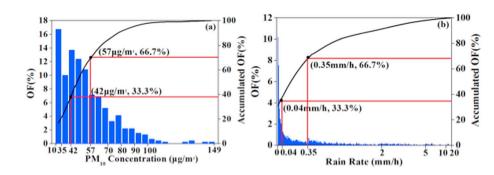|	Bottom Tercile (≤33.3%)	Top Tercile (≥66.7%)
Hourly mean rainfall	$0–0.04\ mm\ h^{-1}$	$0.35–20\ mm\ h^{-1}$
Precipitation intensity	Light	Heavy
Number of hours	1584	1584

Figure 3. Probability density functions of ranked (a) daily PM_{10} concentrations and (b) hourly rain rates during the summer seasons of 2008–2012 over the PRD region. Black solid lines denote accumulated occurrence frequencies for the two data sets (ordinate on the right-hand side of each panel). Red lines show the top and bottom terciles.

although temperature adjustments in radiosonde observations have been made [*Haimberger et al.*, 2008]. The adjustments were derived using analysis departure statistics from ECMWF operational analyses [*Dee et al.*, 2011].

The factor ω plays a significant role in precipitation [*Rose and Lin*, 2003]. Negative and positive ω values correspond to ascent and descent, respectively. The factor ω most closely characterizes the large-scale lift or aggregate impact of convective clouds via a convective parameterization. Caution should be exercised when attributing features of the data to the real dynamic environment involved in cloud formation and development on convective scales. However, the data may be adequate to characterize large-scale forcing over the PRD region ($2° \times 2°$) as a whole because vertical motion from the reanalysis is derived from a combination of observational data and forecast model output [*Dee et al.*, 2011]. Therefore, we have chosen to use this data set to investigate its potential impact on the hourly variation in large-scale precipitation through multiple linear regressions. Three atmospheric layers were chosen for binning ω based upon where clouds and precipitation frequently form: 800–700 hPa, 700–600 hPa, and 600–500 hPa. Mean ω in each bin were calculated so that diurnal variations can be examined. Note that the temporal resolution of this data is 6 h.

Vertical wind shear in the lowest 6 km above ground level (agl) is often thought to be vital for dictating aerosol-cloud-precipitation interactions in large-scale storms [*Yu et al.*, 2010; *Gryspeerdt et al.*, 2014]. Therefore, the bulk shear, S, which refers to the magnitude of the bulk vector difference (top minus bottom) divided by depth [*Thompson et al.*, 2007], was used in the study mainly for characterizing the correlation between large-scale precipitation and aerosols in the multiple linear regression analysis presented in section 3.4. The equation used to calculate S is

$$S = \left(\sqrt{(\overline{u}_{5.5} - \overline{u}_{1.5})^2 + (\overline{v}_{5.5} - \overline{v}_{1.5})^2} \right) / (5500 - 1500), \tag{2}$$

where $\overline{u}_{5.5}$ and $\overline{v}_{5.5}$ represent the average wind speeds in the u and v directions at an altitude of 5500 km and $\overline{u}_{1.5}$ and $\overline{v}_{1.5}$ represent the average wind speeds in the u and v directions at an altitude of 1500 m.

To separate the individual contributions of air pollution, lightning, and meteorological factors to the diurnal variation in heavy precipitation, a standard multiple linear regression was used.

3. Results and Discussion

3.1. Diurnal Variations in Precipitation, Lightning, and Air Pollution

Figure 4 shows the diurnal variations in domain-averaged precipitation amount, lightning density, occurrence frequency of precipitation and lightning strikes, and PM_{10} and NO_2 concentrations over the PRD region. Positive anomalies in the amount and frequency of precipitation and lightning activity begin around 1300 BJT, peak between 1400 and 1700 BJT, then level off until 2100 BJT when negative anomalies appear (Figures 3a and 3b), corroborating the previous finding that both precipitation and lightning flashes in the contiguous southeastern part of China have an afternoon peak during warm seasons [*Xu and Zipser*, 2011]. The surface air temperature often reaches a maximum in the afternoon and the atmosphere in the lower troposphere tends to be unstable over this area in warm seasons. The atmospheric profile is favorable for the generation and development of convective activity and lightning.
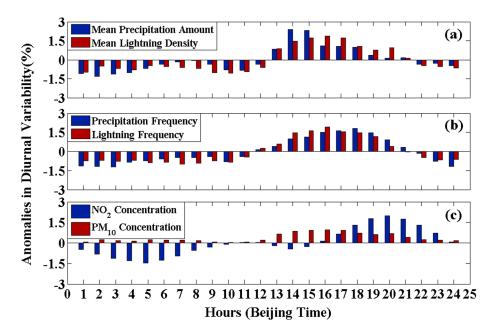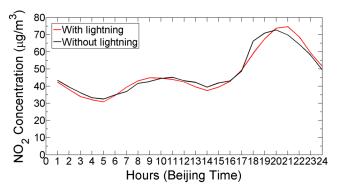
Figure 4. The diurnal variability of anomalies in (a) domain-averaged mean precipitation amount and mean lightning density, (b) domain-accumulated precipitation and lightning frequency over the PRD region during the summer seasons of 2008–2012, and (c) NO_2 and PM_{10} concentrations during two summer seasons (2011–2012). The amplitude anomalies are calculated relative to their 24 h means.

Relatively high peaks in PM_{10} and NO_2 concentrations also occur in the afternoon-to-evening period (Figure 4 c). Normally, the nocturnal boundary layer height (NBLH) is suppressed due to the temperature inversion, which leads to stable atmospheric conditions. The NBLH, in turn, suppresses PM_{10} diffusion in the vertical direction, so PM_{10} concentrations are elevated at night. However, a peak in PM_{10} concentration is seen in the afternoon, coincident with peaks in lightning and precipitation. The observed afternoon peak in aerosol pollution is most likely due to the collective output from anthropogenic (e.g., vehicular traffic) and industrial activities. In theory, a peak in PM_{10} concentration should not appear in the afternoon because of the washout effect caused by the simultaneously occurring convective precipitation. The fact that a peak is seen suggests that the aerosol indirect effect on precipitation/lightning may be at play, although the possibility of natural variability in precipitation and convective available potential energy (CAPE) cannot be ruled out.

Lightning is considered to be an important but uncertain natural source of NO_x. Although it is estimated to be the source of about 5–10% of present-day global tropospheric NO_x [*Jaegle et al.*, 2005], both satellite [*Sioris et al.*, 2007; *Virts et al.*, 2011] and ground-based instruments [*Fraser et al.*, 2007] capture well the enhanced NO_2 following enhanced lightning activities. Figures 4b and 4c show that in the middle of the day when, presumably, there is less traffic on the roads and when lightning would start producing NO_2, concentrations of NO_2 in the air are either constant or decrease. Other anthropogenic emissions into the boundary layer may account for this. The NO_2 peak lags several hours behind the strong lightning strikes in the late afternoon (Figure 4c), contrary to negative NO_2 anomalies occurring during the rush hours in the morning, which is consistent with the lower frequency of lightning and precipitation then. It has been well recognized that the bulk of NO_2 forms quickly from emissions from

Figure 5. The diurnal variation in ground-based in situ measured NO_2 concentration over the PRD during the days with lightning (in red) and the days without lightning (in black).
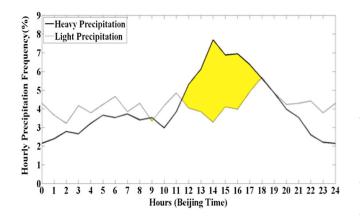
Figure 6. Diurnal variations in heavy (black line) and light (gray line) precipitation accumulated occurrence frequencies, represented as ratios of their corresponding heavy and light precipitation occurrence frequency at a given hour to those accumulated over 24 h, for the summer seasons of 2008–2012 over the PRD region. The yellow shaded area shows when the occurrence frequency of heavy precipitation was larger than that of light precipitation. The amplitude anomalies are calculated relative to their 24 h means.

cars, trucks and buses, power plants, and off-road equipment during rush hours in urban areas like the PRD region. By contrast, the enhanced NO_2 generated during thunderstorms can be detected 1–10 days later at altitudes ranging from 2 to 12 km, depending on the geographical location [*Schumann and Huntrieser*, 2007]. The time scale when lightning-induced NO_2 is transported to the boundary layer can be on the order of minutes to hours, based on the abovementioned estimated propagation speed.

To see if the NO_2 peak in the evening is related to lightning flashes, the diurnal variation in NO_2 is differentiated between days with and without lightning. As shown in Figure 5, NO_2 reaches a peak at 2100 BJT for cases with thunderstorms (lightning), compared with 2000 BJT for cases without thunderstorm (lightning). We may thus infer that the roughly 1 h delay is likely a combination of lightning and human-induced changes in NO_2. Given that the PRD region is heavily polluted and that most of the NO_2 likely comes from anthropogenic activities, the larger than normal peaks in NO_2 concentrations observed in late afternoon to evening are likely caused by anthropogenic emissions as well. As such, to determine the exact contributions from lightning and anthropogenic activities to the peak in NO_2 would require much more state-of-the-art knowledge about the formation processes of NO_2 in the boundary layer than can be provided by the ground-based measurements used here. Model simulations would also help. So the phenomenon shown in Figure 4c suggests that the diurnal cycle of NO_2 is only partially linked to lightning.

3.2. Diurnal Variations in Precipitation Under Clean and Polluted Conditions

Data were further divided according to precipitation intensity. Separate statistical analyses were done on each group of data (Figure 6). The yellow colored area highlights the time of day when heavy precipitation occurred more frequently than light precipitation, i.e., from 1200 BJT to 1800 BJT. This is likely due to the instability of the atmosphere mainly caused by continuous surface heating from solar radiation and the moist atmospheric environment present during that time period. Light precipitation does not show any distinct diurnal cycle.

Figures 7a and 7b shows diurnal variations in mean hourly precipitation amount and occurrence frequency under clean and polluted conditions. From midnight to 1300 BJT, hourly mean precipitation amounts and occurrence frequencies under clean conditions are greater than those under polluted conditions. Among other factors, the radiative effect of enhanced aerosol particles could in part lead to the observed suppression of precipitation. From 1300 BJT to midnight, the trend is reversed, which most likely is due to concurrent changes in radiative and microphysical effects of aerosols, in combination with the CAPE. In the afternoon, the CAPE generally increases and convection develops. The increase in the CAPE through the afternoon comes largely from the continued input of solar radiation at the surface, which is still pronounced until 2, 3, even 4 P.M. and thus lead to atmospheric instability. These are favorable conditions under which the microphysical effect of aerosols comes into play. The pent-up instability could become sufficient to overcome the stabilizing tendency of aerosol direct forcing to allow for the (delayed) initiation of deep convection. Meanwhile, a diurnal cycle exists in competition between the radiative and microphysical effects, as indicated in the full-fledged CSRM model simulation of Part II. That is to say, as the sun sets, the direct radiative effect of aerosols leading to the suppression of convection gives way to the microphysical effect of aerosols, thus leading to invigoration and to the observed phenomenon. However, the evidence concerning the radiative and invigoration effects of aerosols presented so far is circumstantial and requires affirmation from model analyses using a CSRM, which is addressed in Part II.
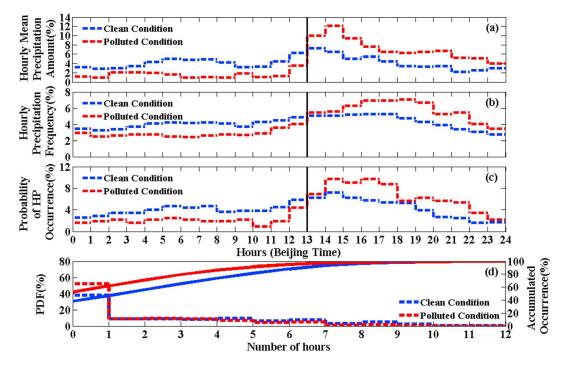
Figure 7. Diurnal variations in (a) hourly mean precipitation amount, (b) accumulated precipitation frequency, and (c) heavy precipitation occurrence frequency, represented as ratios of their corresponding precipitation amount, precipitation frequency, heavy precipitation occurrence frequency at a given hour to those accumulated over 24 h, under clean (blue dashed lines) and polluted (red dashed lines) conditions during the summer seasons of 2008–2012 over the PRD region. The PDFs of the number of hours with (d) heavy precipitation are shown separately under clean (blue lines) and polluted (red lines) conditions, which is calculated based on precipitation data from 1200 to 2400 BJT. The amplitudes in Figures 7a–7c are normalized using the maximum divided by the 24 h sum under clean and polluted conditions. The time when pollution level-dependent patterns in heavy precipitation switch is shown by the black vertical line.

To further inspect the diurnal variations in light and heavy precipitation under clean and polluted conditions, the number of hours with heavy and light precipitation was calculated separately for clean and polluted days. Figure 7c shows that heavy precipitation under polluted conditions tends to occur more frequently from 1300 BJT to 2400 BJT when the atmosphere is more unstable over the PRD region. Under clean conditions, the occurrence frequency of heavy precipitation reaches a peak value at 1400 BJT, then decreases gradually until midnight. The smaller precipitation occurrence frequency before 14:00 BJT (possibly due to suppression by aerosol pollution) is followed by more precipitation in the afternoon and into the night (possibly due to aerosol invigoration), corroborating the theory hypothesized by *Rosenfeld et al.* [2008] with regard to heavy precipitation invigoration in such environments. This is also consistent with the modeling results of *Fan et al.* [2013]. An increase in the number of aerosol particles may alter cloud microphysics by generating more, but smaller, droplets. These droplets suppress the collection/coalescence process, leading to the enhanced release of latent heat as more cloud liquid is transported above the freezing level and the destabilization of the atmosphere. Heavy precipitation is then further invigorated [*Wang et al.*, 2011; *Lee*, 2012]. Also, reduced cloud droplet sizes in warm clouds increase the surface-to-volume ratio of droplets, which, in turn, increases the evaporation efficiency. The increase in the surface-to-volume ratio of droplets not only enhances the evaporation efficiency but also enhances the condensation efficiency. This enhancement of the condensation efficiency results in increases in condensation and associated updrafts, which, in turn, contributes to invigoration [*Koren et al.*, 2014].

The presence of GCCN advected to the study region by the land-sea circulation could be another possible factor explaining the invigoration of heavy precipitation given the close proximity of the South China Sea. As demonstrated by *Rosenfeld et al.* [2002], large sea salt nuclei can override the precipitation suppression effect of a large number of small pollution nuclei over land, leading to efficient warm rain processes.

No obvious pattern in the diurnal cycle of the occurrence frequency of light precipitation is seen (not shown). The quite different observation-based results are consistent with thematic elements in *Tao et al.* [2012] concerning how the impacts of aerosols on shallow and deep convection are expected to differ greatly from
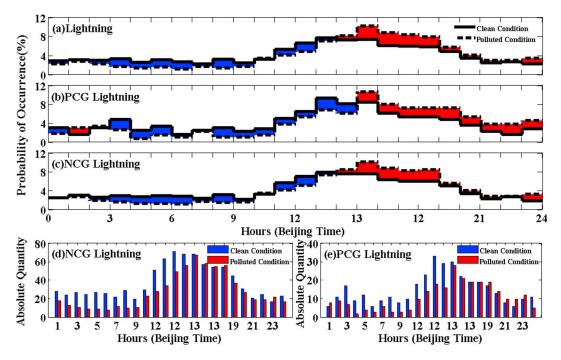
Figure 8. Diurnal variations in (a) lightning frequency, (b) positive cloud-to-ground (PCG) lightning frequency, and (c) negative cloud-to-ground (NCG) lightning frequency, represented as ratios of their corresponding occurrence frequency at a given hour to those accumulated over 24 h, under clean (black solid line) and polluted (black dashed line) conditions for the summer seasons of 2008–2012 over the PRD region. Red areas show the time periods when the lightning occurrence frequency under polluted conditions is greater than that under clean conditions. Blue areas show the time periods when the lightning occurrence frequency under clean conditions is greater than that under polluted conditions. The absolute quantities of (d) NCG and (e) PCG are shown as well.

each other. Note that heavy precipitation is typically assumed to be more closely associated with the presence of deep convection, whereas light precipitation is associated with the presence of warm shallow convection. Due to the heavy precipitation mainly taking place during the afternoon-to-evening period as opposed to other hours of the day, PDFs of the number of hours when heavy precipitation was happening and their accumulated occurrence frequencies from noon to midnight under clean and polluted conditions were constructed (Figure 7d). More heavy precipitation events lasting less than an hour occur under polluted conditions and are likely caused by strong convective storms, indicating polluted storms tend to be shorter in duration. To sum it all up, it rains harder and more frequently, whereas the rain's duration (amount) is shorter (greater) under polluted conditions as compared to those under clean conditions during afternoon hours.

3.3. Diurnal Variation in Lightning Frequency Under Clean and Polluted Conditions

It is commonly acknowledged that lightning is closely associated with convective intensity because the combination of supercooled water and ice crystals, particularly the intensity or rate of riming of supercooled water onto graupel or hail particles, tends to generate charge separation and the electrification of convection [*Williams et al.*, 1991]. Many observational studies point to aerosol particles enhancing lightning [*Rosenfeld et al.*, 2007; *Khain et al.*, 2008; *Bell et al.*, 2009; *Yuan et al.*, 2011]. However, the exact relationship between aerosol concentration and the understanding of cloud electrification in general, and the production of PCG/NCG lightning in particular, is not as well established. Some studies, though, have shown enhanced PCGs in storms that ingest smoke from fires [*Lyons et al.*, 1998; *Vonnegut et al.*, 1995].

Figure 8 shows hourly variations in CG lightning frequencies and occurrence frequencies of PCG/NCG lightning under clean and polluted conditions. The occurrence frequency of lightning flashes under polluted conditions is greater than that under clean conditions from 1400 BJT to midnight (Figure 8a). To some degree, this pattern is similar to the pattern seen in the frequency of heavy precipitation (Figure 7c). Lightning frequencies under polluted conditions were divided into their PCG and NCG components (Figures 8b and 8c). While the pattern of the frequency of NCG lightning is similar to that
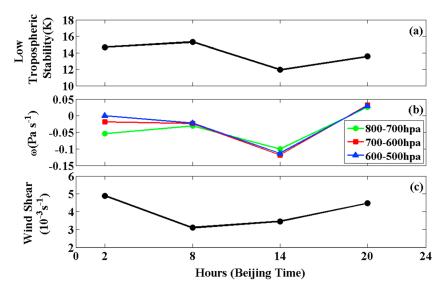
Figure 9. Diurnal variations in (a) lower tropospheric stability, (b) vertical velocity (ω), and (c) vertical wind shear for the summer seasons of 2008–2012 over the PRD region. Data are from the matched 6-hourly ERA-Interim reanalysis data set.

of the all-lightning type (Figure 8a), PCG lightning is enhanced from 1500 BJT until local midnight under more polluted conditions.

Diurnal variations in average absolute numbers of NCG and PCG lightning strikes are shown in Figures 9d and 9e, respectively. Before 1500 BJT, the number of NCG and PCG lightning strikes under clean conditions is greater than that under polluted conditions. After 1500 BJT, the number of NCG and PCG lightning strikes under clean and polluted conditions is comparable, likely because both radiative and microphysical effects of aerosols come into play. Also, the PCG peak timing shown in Figure 8d under polluted conditions (1500 BJT) is delayed by about 2 h compared with that under clean conditions (1300 BJT), as is the NCG peak timing (Figure 8e). Overall, this is consistent with the diurnal variation in lightning frequency.

Also, based on the observations presented in Figure 8e, it would appear that PCGs under polluted conditions occur roughly 30% of the time. This is in good agreement with the percentage (30%) of PCGs observed over the central U.S. during a pollution episode when smoke was transported to the region from massive fires in Mexico [*Lyons et al.*, 1998], which was triple the climatological norm (~10%) over the central U.S.

The possible physical mechanism behind these patterns is somewhat analogous to that of heavy precipitation. Aerosol particles can usually be activated as CCN. Elevated CCN concentrations result in a greater number of smaller droplets, which suppresses warm rain in the lower troposphere and leads to the enhanced release of latent heat at higher altitudes. As a consequence, the higher glaciation height further invigorates the active mixed-phase process [*Yuan et al.*, 2011]. The active mixed-phase process, in turn, affects a myriad of aspects of the charge separation mechanisms [*Williams and Zhang*, 1996; *Brooks et al.*, 1997]. Aside from the dynamic component of aerosol indirect effects, the microphysical component can also impact charge separation without invoking dynamics via latent heat release. According to physical arguments presented in previous studies [e.g., *Takahashi*, 1978; *Williams et al.*, 1991], high CCN levels tend to contribute to high liquid water contents in mixed-phase cloud regions, and subsequently to more positive rimer charging. As shown in laboratory studies [e.g., *Takahashi*, 1978, Figure 8], charge separation per collision was observed to increase as a function of liquid water content for temperatures warmer than about $-10°C$ or $-15°C$ (the charge reversal temperature). The increase in lightning frequency could be the result of simply introducing more liquid into the mixed-phase region because high CCN concentrations contribute to decreases in droplet mean diameter and thus stunt the warm rain process. However, we are unable to differentiate between these two processes with our observations. This will be examined in Part II by model simulations.

3.4. Correlation Analysis

The above inference may not be true if changes in meteorological factors could explain aspects of the diurnal variation in (heavy) precipitation. Further analysis is required regarding the diurnal cycle of multiple

meteorological factors and their possible impacts on precipitation [*Huang et al.*, 2009]. In this section, a few meteorological variables that correlate sufficiently well with the variation in hourly precipitation are examined in an attempt to restrict the meteorological variance at an hourly scale.

3.4.1. Precipitation-Related Weather Factors

Diurnal variations in precipitation and lightning are closely related to large-scale synoptic conditions. ERA-Interim reanalysis data are used to obtain LTS, ω, and vertical wind shear, all of which are at 6-hourly intervals. Observation and model studies have revealed the effects of these meteorological variables on convective precipitation [*Fan et al.*, 2009]. High LTS values generally signify the existence of a strong inversion layer, indicative of a relatively stable atmospheric stratification. Figure 9 shows a minimum in LTS at 1400 BJT, which suggests low atmospheric stability. A smaller value of LTS is more favorable for the development of widespread deep convection due to the more unstable atmospheric column. Figure 9b shows a minimum in mean ω at 1400 BJT at each level examined (500–600 hPa, 600–700 hPa, and 700–800 hPa), which indicates upward motion. The minimum in ω may further facilitate the formation of convection and may result in more precipitation. The maximum in mean precipitation amount at 1400 BJT (Figure 4a) suggests that favorable dynamic conditions for the generation of precipitation were in place then, illustrating that it is difficult to isolate aerosol effects from thermodynamic and dynamic effects when it comes to the observed diurnal features of precipitation over the PRD region. The phenomenon observed here reiterates the need to perform further detailed statistical analyses, in combination with model simulations.

Vertical wind shear is another meteorological variable at play in the generation and development of convective precipitation. Figure 9c shows that a weaker wind shear occurs at 1400 BJT, coincident with maxima in precipitation amount and frequency (Figures 4a and 4b). This is in good agreement with the findings in *Fan et al.* [2009] that increasing aerosol concentrations have been thought to enhance convection (more precipitation amount) under weak wind shear conditions, which is probably highly dependent on location. A precipitation efficiency metric (e.g., the ratio of precipitation amount to condensate amount) would be more instructive. Investigating this statistic at different points in the domain versus considering a domain-wide average might yield clues as to what is going on. This is a direction for future research. Given the above inconsistency between observational and model results, a further check on whether vertical wind shear could dictate the diurnal variation in precipitation is needed. This meteorological factor will be included in the following multiple regression analyses.

3.4.2. Multiple Linear Regression of Various Factors Onto Heavy Precipitation

Given the analysis results in section 3.4.1, the heavy precipitation (predictand) is regressed onto multiple predictor variables such as PM_{10}, NO_2, LTS, ω, and S using multiple linear regression models. As such, the impact of weather-related factors on the hourly variation in heavy precipitation events is expected to be statistically determined. Furthermore, the six variables selected have been standardized prior to a regression of this kind to facilitate an "apples-to-apples" comparison of the relative weight assigned to individual independent predictors.

Typically speaking, the multiple regression model estimates of the coefficients become unstable and the standard errors for the coefficients can get wildly inflated, with the increasing degree of multicollinearity. The variance inflation factor (VIF) has been widely used as a measure of the degree of multicollinearity of the ith predictor variable with the rest of predictor set. The VIF is generally formulated as $VIF = 1/(1-R_i^2)$, where R_i^2 denotes the determination coefficient. In practice, VIFs exceeding some threshold values are the signs of multicollinearity, making it very difficult to unequivocally attribute the explained variance of the predicted variable to any individual predictor alone. A spectrum of rules of thumb for threshold values of VIF has appeared in literatures, including the rule of 5 [e.g., *Menard*, 1995] and the rule of 10 [e.g., *Hair et al.*, 1995]. In order to test whether there exists multicollinearity among the multiple predictor variables, VIF has been calculated before applying the forward selection routines. Although all of the VIF values for the independent predictors in this study do not exceed 5, the linear dependences among the independent predictors are still nontrivial, given VIF as an indicator, among other important statistical indices, of potential complications that may arise from the presence of multicollinearity [*O'brien*, 2007]. More promising are the daily results compared with those at 0200, 0800, 1400, and 2000 BJT in terms of the apparent lack of multicollinearity.

The forward selection technique described in previous textbooks [e.g., *Draper and Smith*, 1998; *Montgomery et al.*, 2001; *Wilks*, 2011] was used to select a good set of predictors from a pool of potential predictors in the multiple linear regression analyses. Because lightning has a strong association with precipitation [e.g., *Carey and Rutledge*, 2000; *Pessi and Businger*, 2009], it will not be included in the following multiple linear regression

Table 3. Summary of Statistics of the Forward Selection Procedure for the Development of a Regression Equation for Heavy Precipitation Based on the Five Potential Predictors[a]

Time (BJT)	K	Predictors Entered	R^2	Standard Error	MSE	F	p	Coefficient
0800	1	PM_{10}	0.67	0.05	6.82	4.97	0.04	−0.01
		Model: Heavy precipitation = $-0.01\,PM_{10} + 5.49$						
1400	1	$\overline{\omega}$	0.61	0.02	2.95	4.81	0.04	−0.33
	2	PM_{10}	0.64	0.04	2.73	5.33	0.03	−0.04
	3	LTS	0.68	0.11	2.66	5.36	0.02	0.28
		Model: Heavy precipitation = $-0.33\overline{\omega} - 0.04\,PM_{10} + 0.28\,LTS + 11.58$						
Daily	1	PM_{10}	0.53	0.03	3.92	4.07	0.04	−0.01
		Model: Heavy precipitation = $-0.01\,PM_{10} + 6.56$						

[a]At each step, the variable producing the best predictions in the multiple regression equation is chosen, whose standard squared error (MSE), R, standard error, p value, F ratio, and estimates of multiple correlation coefficients for the regression as a whole are given as well.

analyses. Multiple linear models of heavy precipitation regressed against various factors at 0200, 0800, 1400, and 2000 BJT and their daily averages are constructed.

The results of progressive iterations of the forward selection routines are listed in Table 3. The coefficient estimates applied to each individual predictor, standard error estimates for each predictor, multiple correlation coefficients, and F statistics are shown for each iteration. At each step ($K = 1, 2, 3…$), the variable producing the best predictions in the multiple regression equation is chosen. As such, the predictors selected through the abovementioned progressively iterative processes varied temporally, i.e., PM_{10} for both 0800 BJT and the daily average, in contrast to PM_{10}, LTS, and $\overline{\omega}$ at 1400 BJT. In particular, the step of $K = 2$ at 1400 BJT, when both PM_{10} and $\overline{\omega}$ are selected as predictor variables, illustrates a marginal increase in R^2 by roughly 5%, indicating that the two variables describe some different portions of variance in the response of heavy precipitation. The step of $K = 3$, when LTS is selected as predicator variable, does not increase R^2 dramatically. Furthermore, the F ratio increases and the mean squared error (MSE) decreases with forward stepping from $K = 1$ to $K = 2$ and to $K = 3$, implying that the multiple regression model including aerosols, thermodynamics, and dynamics better describes the response than either factor does separately.

By and large, PM_{10}, compared with other factors, seems to be a more reliable predictor for heavy precipitation due to its ubiquitous presence in the multiple regression models at 0800 BJT, 1400 BJT, and daily average. The multiple regression results further suggest that heavy precipitation over the PRD region during the summer season is most closely associated with air pollution and that the indirect effects of anthropogenic aerosols on precipitation are significant and cannot be dismissed.

4. Conclusions

The impact of aerosols on precipitation and thunderstorms has been reported in many previous studies, but little is known about their impact on diurnal variations in precipitation and thunderstorms. Given that there are radiative and microphysical aerosol effects, the possibility that aerosols have an impact on these diurnal variations is envisioned, but not established as yet. In principle, the aerosol radiative effect suppresses convection, while the invigoration effect strengthens it. Because the former effect decreases toward sunset, a delay in peak thunderstorm activity with increasing aerosol loading is expected.

To test the above hypothesis, extensive data analyses were conducted using data collected in the PRD region in south China where pollution is typically heavy. Long-term meteorological and air pollution data sets collected during the summer seasons (June to August) of 2008–2012 were analyzed. Data sets include hourly CMORPH precipitation data, lightning strike measurements from 14 sites, 6-hourly ERA-Interim reanalysis data, and hourly NO_2 and PM_{10} measurements from 19 sites spread across the PRD region. Results show that precipitation and lightning activities reach peak values during the hours of 1400–1700 BJT in terms of both amount and frequency of occurrence. This is also when PM_{10} concentrations are at their highest.

To examine the possible effect of aerosols on precipitation and lightning, the top and bottom PM_{10} terciles were selected to represent polluted and clean subsets of data. Also, these separate data subsamples were required to be equal in number so that the resulting differences are more likely to be indicative of robust

patterns in the data, as opposed to those caused by chance. Typically, precipitation and lightning occur more frequently in the afternoon to evening hours than in the rest of the day. Diurnal variations in both quantities are more striking under polluted conditions than under clean conditions. Two tipping points when a switch in pollution level-dependent patterns in heavy precipitation occurs are identified, namely, 1300 BJT and 2400 BJT. Before 1300 BJT, rainfall and lightning occur more often under clean conditions than under polluted conditions. From 1300 to 2400 BJT, the precipitation amount and frequency tend to be much greater under polluted conditions than under clean conditions. The same holds for lightning flashes. Under polluted conditions, the occurrence frequency of lightning was enhanced from 1500 BJT to midnight. After 2400 BJT, the trends were reversed, i.e., less precipitation and less lightning occurring under polluted conditions than under clean conditions, presumably because of the greater amount of energy consumed through the generation of more precipitation in the several preceding hours under polluted conditions.

The correlation analyses were performed between heavy precipitation and three meteorological variables at 6-hourly intervals (LTS, ω, and vertical wind shear) that correlate well with precipitation, in an attempt to determine whether they have the same diurnal cycles as heavy precipitation. With a focus on 1300 BJT, which is when aerosol concentrations, lightning, and heavy precipitation peak, LTS and ω provide favorable conditions for the development of precipitation, whereas wind shear tends to suppress it. The overall effect of aerosol and meteorology on precipitation is examined by performing multiple linear regression analyses. Although the effect of aerosol particles can be discernible on the heavy precipitation through the daytime, the influence of concurrent atmospheric dynamics and thermodynamics cannot be ruled out, which merits further investigation in the future.

References

Albrecht, B. A. (1989), Aerosols, cloud microphysics, and fractional cloudiness, *Science*, 245(4923), 1227–1230.

Altaratz, O., I. Koren, Y. Yair, and C. Price (2010), Lightning response to smoke from Amazonian fires, *Geophys. Res. Lett.*, 37, L07801, doi:10.1029/2010GL042679.

Anderson, T. L., R. J. Charlson, D. M. Winker, J. A. Ogren, and K. Holmen (2003), Mesoscale variations of tropospheric aerosols, *J. Atmos. Sci.*, 60, 119–136, doi:10.1175/1520-0469(2003)060<0119:mvota>2.0.co;2.

Andreae, M. O. (2009), Correlation between cloud condensation nuclei concentration and aerosol optical thickness in remote and polluted regions, *Atmos. Chem. Phys.*, 9(2), 543–556.

Andreae, M. O., D. Rosenfeld, P. Artaxo, A. A. Costa, G. P. Frank, K. M. Longo, and M. A. F. Silva-Dias (2004), Smoking rain clouds over the Amazon, *Science*, 303(5662), 1337–1342, doi:10.1126/science.1092779.

Avila, E. E., R. G. Pereyra, G. G. Aguirre Varela, and G. M. Caranti (1999), The effect of the cloud droplet spectrum on electrical-charge transfer during individual ice-ice collisions, *Q. J. R. Meteorol. Soc.*, 125, 1669–1679.

Baker, M. B., and J. G. Dash (1994), Mechanism of charge transfer between colliding ice particles in thunderstorms, *J. Geophys. Res.*, 99, 10,621–10,626, doi:10.1029/93JD01633.

Basu, B. K. (2007), Diurnal variation in precipitation over India during the summer monsoon season: Observed and model predicted, *Mon. Weather Rev.*, 135(6), 2155–2167, doi:10.1175/mwr3355.1.

Bäumer, D., and B. Vogel (2007), An unexpected pattern of distinct weekly periodicities in climatological variables in Germany, *Geophys. Res. Lett.*, 34, L03819, doi:10.1029/2006GL028559.

Bell, T. L., D. Rosenfeld, and K. M. Kim (2009), Weekly cycle of lightning: Evidence of storm invigoration by pollution, *Geophys. Res. Lett.*, 36, L23805, doi:10.1029/2009GL040915.

Brooks, I. M., C. P. R. Saunders, R. P. Mitzeva, and S. L. Peck (1997), The effect on thunderstorm charging of the rate of rime accretion by graupel, *Atmos. Res.*, 43(3), 277–295, doi:10.1016/S0169-8095(96)00043-9.

Carey, L. D., and S. A. Rutledge (2000), The relationship between precipitation and lightning in tropical island convection: A C-band polarimetric radar study, *Mon. Weather Rev.*, 128, 2687–2710, doi:10.1175/1520-0493(2000)128<2687:TRBPAL>2.0.CO;2.

Chen, M. L., T. Lu, and Y. P. Du (2011), Performance of TOA/DF lightning location network in China—Site errors and detection efficiency, paper presented at 7th Asian-Pacific International Conference on Lightning, IEEE, Chengdu, China.

Christian, H. J., et al. (2003), Global frequency and distribution of lightning as observed from space by the Optical Transient Detector, *J. Geophys. Res.*, 108(D1), 4005, doi:10.1029/2002JD002347.

Dee, D. P., et al. (2011), The ERA-Interim reanalysis: Configuration and performance of the data assimilation system, *Q. J. R. Meteorol. Soc.*, 137(656), 553–597, doi:10.1002/qj.828.

Draper, N. R., and H. Smith (1998), *Applied Regression Analysis*, 3rd ed., Wiley, New York.

Fan, J., T. Yuan, J. M. Comstock, S. Ghan, A. Khain, L. R. Leung, Z. Li, V. J. Martins, and M. Ovchinnikov (2009), Dominant role by vertical wind shear in regulating aerosol effects on deep convective clouds, *J. Geophys. Res.*, 114, D22206, doi:10.1029/2009JD012352.

Fan, J., L. R. Leung, D. Rosenfeld, Q. Chen, Z. Li, J. Zhang, and H. Yan (2013), Microphysical effects determine macrophysical response for aerosol impact on deep convective clouds, *Proc. Natl. Acad. Sci. U.S.A.*, 110, E4581–E4590, doi:10.1073/pnas.1316830110.

Feng, S., Q. Hu, and W. Qian (2004), Quality control of daily meteorological data in China, 1951–2000: A new dataset, *Int. J. Climatol.*, 24(7), 853–870, doi:10.1002/joc.1047.

Forster, P., et al. (2007), Changes in atmospheric constituents and in radiative forcing, in *Contribution of Working Group I to the Fourth Assessment Report of the Intergovernmental Panel on Climate Change. Climate Change 2007: The Physical Science Basis*, edited by S. Solomon et al., pp. 129–234, Cambridge Univ. Press, Cambridge, U. K.

Fraser, A., F. Goutail, C. A. McLinden, S. M. L. Melo, and K. Strong (2007), Lightning-produced NO$_2$ observed by two ground-based UV-visible spectrometers at Vanscoy, Saskatchewan in August 2004, *Atmos. Chem. Phys.*, 7, 1683–1692, doi:10.5194/acp-7-1683-2007.

Fu, C., and L. Dan (2014), Trends in the different grades of precipitation over South China during 1960–2010 and the possible link with anthropogenic aerosols, *Adv. Atmos. Sci.*, *31*(2), 480–491, doi:10.1007/s00376-013-2102-7.

Fujibe, F. (1999), Diurnal variation in the frequency of heavy precipitation in Japan, *J. Meteorol. Soc. Jpn.*, *77*(6), 1137–1149.

Givati, A., and D. Rosenfeld (2004), Quantifying precipitation suppression due to air pollution, *J. Appl. Meteorol.*, *43*(7), 1038–1056, doi:10.1175/1520-0450(2004)043<1038:qpsdta>2.0.co;2.

Gryspeerdt, E., P. Stier, and D. G. Partridge (2014), Satellite observations of cloud regime development: The role of aerosol processes, *Atmos. Chem. Phys.*, *14*(3), 1141–1158.

Guo, J., X. Y. Zhang, Y. R. Wu, Y. Zhaxi, H. Z. Che, B. La, W. Wang, and X. W. Li (2011), Spatio-temporal variation trends of satellite-based aerosol optical depth in China during 1980–2008, *Atmos. Environ.*, *45*(37), 6802–6811, doi:10.1016/j.atmosenv.2011.03.068.

Guo, J., M. Deng, J. Fan, Z. Li, Q. Chen, P. Zhai, Z. Dai, and X. Li (2014a), Precipitation and air pollution at mountain and plain stations in northern China: Insights gained from observations and modeling, *J. Geophys. Res. Atmos.*, *119*, 4793–4807, doi:10.1002/2013JD021161.

Guo, J., P. Zhai, L. Wu, M. Cribb, Z. Li, Z. Ma, F. Wang, D. Chu, P. Wang, and J. Zhang (2014b), Diurnal variation and the influential factors of precipitation from surface and satellite measurements in Tibet, *Int. J. Climatol.*, *34*, 2940–2956, doi:10.1002/joc.3886.

Haimberger, L., C. Tavolato, and S. Sperka (2008), Toward elimination of the warm bias in historic radiosonde temperature records—Some new results from a comprehensive intercomparison of upper-air data, *J. Clim.*, *21*, 4587–4606, doi:10.1175/2008JCLI1929.1.

Hair, J. F., Jr., R. E. Anderson, R. L. Tatham, and W. C. Black (1995), *Multivariate Data Analysis*, 3rd ed., Macmillan, New York.

Hidayat, S., and M. Ishii (1999), Diurnal variation of lightning characteristics around Java Island, *J. Geophys. Res.*, *104*, 24,449–24,454, doi:10.1029/1999JD900769.

Huang, J., C. Zhang, and J. M. Prospero (2009), Aerosol-induced large-scale variability in precipitation over the tropical Atlantic, *J. Clim.*, *22*(19), 4970–4988, doi:10.1175/2009jcli2531.1.

Jaegle, L., L. Steinberger, R. V. Martin, and K. Chance (2005), Global partitioning of NO_x sources using satellite observations: Relative roles of fossil fuel combustion, biomass burning and soil emissions, *Faraday Discuss.*, *130*, 407–423, doi:10.1039/b502128f.

Jayaratne, E. R. (1993), The heat balance of a riming graupel pellet and the charge separation during ice–ice collisions, *J. Atmos. Sci.*, *50*, 3185–3193.

Khain, A., N. Cohen, B. Lynn, and A. Pokrovsky (2008), Possible aerosol effects on lightning activity and structure of hurricanes, *J. Atmos. Sci.*, *65*(12), 3652–3677, doi:10.1175/2008jas2678.1.

Koren, I., Y. J. Kaufman, L. A. Remer, and J. V. Martins (2004), Measurement of the effect of Amazon smoke on inhibition of cloud formation, *Science*, *303*(5662), 1342–1345, doi:10.1126/science.1089424.

Koren, I., J. V. Martins, L. A. Remer, and H. Afargan (2008), Smoke invigoration versus inhibition of clouds over the Amazon, *Science*, *321*(5891), 946–949, doi:10.1126/science.1159185.

Koren, I., G. Feingold, and L. A. Remer (2010), The invigoration of deep convective clouds over the Atlantic: Aerosol effect, meteorology or retrieval artifact?, *Atmos. Chem. Phys.*, *10*(18), 8855–8872, doi:10.5194/acp-10-8855-2010.

Koren, I., O. Altaratz, L. A. Remer, G. Feingold, J. V. Martins, and R. H. Heiblum (2012), Aerosol-induced intensification of rain from the tropics to the mid-latitudes, *Nat. Geosci.*, *5*, 118–122, doi:10.1038/ngeo1364.

Koren, I., G. Dagan, and O. Altaratz (2014), From aerosol-limited to invigoration of warm convective clouds, *Science*, *344*(6188), 1143–1146, doi:10.1126/science.1252595.

Kucienska, B., G. B. Raga, and R. Romero-Centeno (2012), High lightning activity in maritime clouds near Mexico, *Atmos. Chem. Phys.*, *12*(17), 8055–8072, doi:10.5194/acp-12-8055-2012.

Lee, S. S. (2012), Effect of aerosol on circulations and precipitation in deep convective clouds, *J. Atmos. Sci.*, *69*, 1957–1974.

Levin, Z., and W. R. Cotton (2009), *Aerosol Pollution Impact on Precipitation: A Scientific Review*, 386 pp., Springer, Berlin.

Li, Z., X. Zhao, R. Kahn, M. Mishchenko, L. Remer, K.-H. Lee, M. Wang, I. Laszlo, T. Nakajima, and H. Maring (2009), Uncertainties in satellite remote sensing of aerosols and impact on monitoring its long-term trend: A review and perspective, *Ann. Geophys.*, *27*, 1–16.

Li, Z., F. Niu, J. Fan, Y. Liu, D. Rosenfeld, and Y. Ding (2011), Long-term impacts of aerosols on the vertical development of clouds and precipitation, *Nat. Geosci.*, *4*(12), 888–894, doi:10.1038/ngeo1313.

Liu, C., and E. J. Zipser (2008), Diurnal cycles of precipitation, clouds, and lightning in the tropics from 9 years of TRMM observations, *Geophys. Res. Lett.*, *35*, L04819, doi:10.1029/2007GL032437.

Liu, C., E. R. Williams, E. J. Zipser, and G. Burns (2010), Diurnal variations of global thunderstorms and electrified shower clouds and their contribution to the global electrical circuit, *J. Atmos. Sci.*, *67*(2), 309–323, doi:10.1175/2009JAS3248.1.

Lyons, W. A., T. E. Nelson, E. R. Williams, J. A. Cramer, and T. R. Turner (1998), Enhanced positive cloud-to-ground lightning in thunderstorms ingesting smoke from fires, *Science*, *282*, 77–80, doi:10.1126/science.282.5386.77.

Menard, S. (1995), *Applied Logistic Regression Analysis*, Sage Univ. Ser. on Quant. Appl. in the Soc. Sci., Sage, Thousand Oaks, Calif.

Meng, Q., H. Ding, Y. Zhang, X. Xu, J. Yuan, X. Zhu, W. Yao, and W. Lv (2006), Development of national lightning detection network and its applications in China, World Meteorol. Organ., Natl. Lightning Saf. Inst. [Available at https://www.wmo.int/pages/prog/www/IMOP/publications/IOM-94-TECO2006/P2(04)_Meng-Qing-Mrs_China.pdf. Retrieved 2015-08-06].

Montgomery, D. C., E. A. Peck, and G. G. Vining (2001), *Introduction to Linear Regression Analysis*, Wiley-Interscience, Hoboken, N. J.

O'brien, R. M. (2007), A caution regarding rules of thumb for variance inflation factors, *Qual. Quant.*, *41*(5), 673–690.

Peng, J., Z. Li, H. Zhang, J. Liu, and M. Cribb (2015), Systematic changes in cloud radiative forcing with aerosol loading for deep clouds in the tropics, *J. Atmos. Sci.*, doi:10.1175/JAS-D-15-0080.1.

Pessi, A. T., and S. Businger (2009), Relationships among lightning, precipitation, and hydrometeor characteristics over the North Pacific Ocean, *J. Appl. Meteorol. Climatol.*, *48*, 833–848, doi:10.1175/2008JAMC1817.1.

Qian, Y., D. P. Kaiser, L. R. Leung, and M. Xu (2006), More frequent cloud-free sky and less surface solar radiation in China from 1955 to 2000, *Geophys. Res. Lett.*, *33*, L01812, doi:10.1029/2005GL024586.

Rodwell, M. J., and T. Jung (2008), Understanding the local and global impacts of model physics changes: An aerosol example, *Q. J. R. Meteorol. Soc.*, *134*, 1479–1497.

Rose, B. E. J., and C. A. Lin (2003), Precipitation from vertical motion: A statistical diagnostic scheme, *Int. J. Climatol.*, *23*(8), 903–919.

Rosenfeld, D. (1999), TRMM observed first direct evidence of smoke from forest fires inhibiting rainfall, *Geophys. Res. Lett.*, *26*, 3105–3108, doi:10.1029/1999GL006066.

Rosenfeld, D., and T. L. Bell (2011), Why do tornados and hailstorms rest on weekends?, *J. Geophys. Res.*, *116*, D20211, doi:10.1029/2011JD016214.

Rosenfeld, D., R. Lahav, A. Khain, and M. Pinsky (2002), The role of sea spray in cleansing air pollution over ocean via cloud processes, *Science*, *297*, 1667–1670, doi:10.1126/science.1073869.

Rosenfeld, D., M. Fromm, J. Trentmann, G. Luderer, M. O. Andreae, and R. Servranckx (2007), The Chisholm firestorm: Observed microstructure, precipitation and lightning activity of a pyro-Cb, *Atmos. Chem. Phys. Discuss.*, *6*(5), 9877–9906, doi:10.5194/acpd-6-9877-2006.

Rosenfeld, D., U. Lohmann, G. B. Raga, C. D. O'Dowd, M. Kulmala, S. Fuzzi, A. Reissell, and M. O. Andreae (2008), Flood or drought: How do aerosols affect precipitation?, *Science*, *321*(5894), 1309–1313.

Rosenfeld, D., et al. (2014), Global observations of aerosol-cloud-precipitation-climate interactions, *Rev. Geophys.*, *52*, 750–808, doi:10.1002/2013RG000441.

Saunders, C. P. R. (1994), Thunderstorm electrification laboratory experiments and charging mechanisms, *J. Geophys. Res.*, *99*, 10,773–10,779, doi:10.1029/93JD01624.

Schumann, U., and H. Huntrieser (2007), The global lightning-induced nitrogen oxides source, *Atmos. Chem. Phys.*, *7*, 3823–3907, doi:10.5194/acp-7-3823-2007.

Seinfeld, J. H., and S. N. Pandis (1998), *Atmospheric Chemistry and Physics: From Air Pollution to Climate Change*, 1326 pp., John Wiley, New York.

Shen, Y., P. Zhao, Y. Pan, and J. Yu (2014), A high spatiotemporal gauge-satellite merged precipitation analysis over China, *J. Geophys. Res. Atmos.*, *119*, 3063–3075, doi:10.1002/2013JD020686.

Sioris, C. E., et al. (2007), Vertical profiles of lightning-produced NO_2 enhancements in the upper troposphere observed by OSIRIS, *Atmos. Chem. Phys.*, *7*, 4281–4294, doi:10.5194/acp-7-4281-2007.

Slingo, J. (1987), The development and verification of a cloud prediction scheme for the ECMWF model, *Q. J. R. Meteorol. Soc.*, *113*(477), 899–927.

Sorooshian, S., X. Gao, K. Hsu, R. Maddox, Y. Hong, H. Gupta, and B. Imam (2002), Diurnal variability of tropical rainfall retrieved from combined GOES and TRMM satellite information, *J. Clim.*, *15*(9), 983–1001.

Stolz, D. C., S. A. Rutledge, and J. R. Pierce (2015), Simultaneous influences of thermodynamics and aerosols on deep convection and lightning in the tropics, *J. Geophys. Res. Atmos.*, *120*, 6207–6231, doi:10.1002/2014JD023033.

Storer, R. L., S. C. van den Heever, and T. S. L'Ecuyer (2014), Observations of aerosol-induced convective invigoration in the tropical east Atlantic, *J. Geophys. Res. Atmos.*, *119*, 3963–3975, doi:10.1002/2013JD020272.

Takahashi, T. (1978), Rimming electrification as a charge generation mechanism in thunderstorms, *J. Atmos. Sci.*, *35*(8), 1536–1548, doi:10.1175/1520-0469(1978)035<1536:REAACG>2.0.CO;2.

Tao, W. K., J. P. Chen, Z. Li, C. Wang, and C. D. Zhang (2012), Impact of aerosols on convective clouds and precipitation, *Rev. Geophys.*, *50*, RG2001, doi:10.1029/2011RG000369.

Thompson, R. L., C. M. Mead, and R. Edwards (2007), Effective storm-relative helicity and bulk shear in supercell thunderstorm environments, *Weather Forecasting*, *22*(1), 102, doi:10.1175/WAF969.1.

Tompkins, A. M., C. Cardinali, J.-J. Morcrette, and M. Rodwell (2005), Influence of aerosol climatology on forecasts of the African Easterly Jet, *Geophys. Res. Lett.*, *32*, L10801, doi:10.1029/2004GL022189.

Twohy, C. H., J. A. Coakley Jr., and W. R. Tahnk (2009), Effect of changes in relative humidity on aerosol scattering near clouds, *J. Geophys. Res.*, *114*, D05205, doi:10.1029/2008JD010991.

Twomey, S. (1977), The influence of pollution on the shortwave albedo of clouds, *J. Atmos. Sci.*, *34*(7), 1149–1152, doi:10.1175/1520-0469(1977)034<1149:tiopot>2.0.co;2.

Uppala, S., D. Dee, S. Kobayashi, P. Berrisford, and A. Simmons (2008), Towards a climate data assimilation system: Status update of ERA-Interim, *ECMWF Newsl.*, *115*, 12–18.

Virts, K. S., J. A. Thornton, J. M. Wallace, M. L. Hutchins, R. H. Holzworth, and A. R. Jacobson (2011), Daily and intraseasonal relationships between lightning and NO_2 over the Maritime Continent, *Geophys. Res. Lett.*, *38*, L19803, doi:10.1029/2011GL048578.

Vonnegut, B., D. J. Latham, C. B. Moore, and S. J. Hunyady (1995), An explanation for anomalous lightning from forest fire clouds, *J. Geophys. Res.*, *100*, 5037–5050, doi:10.1029/94JD02956.

Wall, C., E. Zipser, and C. T. Liu (2014), An investigation of the aerosol indirect effect on convective intensity using satellite observations, *J. Atmos. Sci.*, *71*(1), 430–447, doi:10.1175/jas-d-13-0158.1.

Wallace, J. M. (1975), Diurnal variations in precipitation and thunderstorm frequency over the conterminous United States, *Mon. Weather Rev.*, *103*(5), 406–419, doi:10.1175/1520-0493(1975)103<0406:dvipat>2.0.co;2.

Walters, C. K., and J. A. Winkler (1999), Diurnal variations in the characteristics of cloud-to-ground lightning activity in the Great Lakes region of the United States, *Prof. Geogr.*, *51*(3), 349–366, doi:10.1111/0033-0124.00171.

Wang, J., S. C. van den Heever, and J. S. Reid (2009), A conceptual model for the link between Central American biomass burning aerosols and severe weather over the south central United States, *Environ. Res. Lett.*, *4*(1), 015003, doi:10.1088/1748-9326/4/1/015003.

Wang, Y., Q. Wan, W. Meng, F. Liao, H. Tan, and R. Zhang (2011), Long-term impacts of aerosols on precipitation and lightning over the Pearl River Delta megacity area in China, *Atmos. Chem. Phys.*, *11*(23), 12,421–12,436, doi:10.5194/acp-11-12421-2011.

Wilks, D. S. (2011), *Statistical Methods in the Atmospheric Sciences*, vol. 100, Academic, Waltham, Mass.

Williams, E. R., and R. Zhang (1996), Density of rime in laboratory simulations of thunderstorm microphysics and electrification, *J. Geophys. Res.*, *101*, 29,715–29,719, doi:10.1029/96JD03216.

Williams, E. R., R. Zhang, and J. Rydock (1991), Mixed-phase microphysics and cloud electrification, *J. Atmos. Sci.*, *48*(19), 2195–2203, doi:10.1175/1520-0469(1991)048<2195:mpmace>2.0.co;2.

Wood, R., and C. S. Bretherton (2006), On the relationship between stratiform low cloud cover and lower-tropospheric stability, *J. Clim.*, *19*(24), 6425–6432.

Xu, W. X., and E. J. Zipser (2011), Diurnal variations of precipitation, deep convection, and lightning over and east of the eastern Tibetan Plateau, *J. Clim.*, *24*(2), 448–465, doi:10.1175/2010jcli3719.1.

Yang, X., and Z. Li (2014), Increases in thunderstorm activity and relationships with air pollution in southeast China, *J. Geophys. Res. Atmos.*, *119*, 1835–1844, doi:10.1002/2013JD021224.

Yu, J., Z. Tan, and Y. Wang (2010), Effects of vertical wind shear on intensity and rainfall asymmetries of strong Tropical Storm Bilis (2006), *Adv. Atmos. Sci.*, *27*(3), 552–561, doi:10.1007/s00376-009-9030-6.

Yu, R., Y. Xu, T. Zhou, and J. Li (2007), Relation between rainfall duration and diurnal variation in the warm season precipitation over central eastern China, *Geophys. Res. Lett.*, *34*, L13703, doi:10.1029/2007GL030315.

Yuan, T., L. A. Remer, K. E. Pickering, and H. Yu (2011), Observational evidence of aerosol enhancement of lightning activity and convective invigoration, *Geophys. Res. Lett.*, *38*, L04701, doi:10.1029/2010GL046052.

Yuan, T., L. A. Remer, H. Bian, J. R. Ziemke, R. Albrecht, K. E. Pickering, L. Oreopoulos, S. J. Goodman, H. Yu, and D. J. Allen (2012), Aerosol indirect effect on tropospheric ozone via lightning, *J. Geophys. Res.*, *117*, D18213, doi:10.1029/2012JD017723.

Zhang, R., G. Li, J. Fan, D. L. Wu, and M. J. Molina (2007), Intensification of Pacific storm track linked to Asian pollution, *Proc. Natl. Acad. Sci. U.S.A.*, *104*(13), 5295–5299, doi:10.1073/pnas.0700618104.

Zhang, R., Q. Li, and R. Zhang (2014), Meteorological conditions for the persistent severe fog and haze event over eastern China in January 2013, *Sci. China Earth Sci.*, *57*(1), 26–35, doi:10.1007/s11430-013-4774-3.